

Resource-efficient and loss-aware photonic graph state preparation using an array of quantum emitters, and application to all-photonic quantum repeaters

Eneet Kaur,^{1,2,*} Ashlesha Patil,^{1,*} and Saikat Guha¹

¹*Wyant College of Optical Sciences, University of Arizona,
1630 E University Blvd, Tucson, AZ, 85719, USA*

²*Cisco Quantum Lab, Los Angeles, USA*

Multi-qubit photonic graph states are necessary for quantum communication and computation. Preparing photonic graph states using probabilistic stitching of single photons using linear optics results in a formidable resource requirement due to the need of multiplexing. Quantum emitters present a viable solution to prepare photonic graph states, as they enable controlled production of photons entangled with the emitter qubit, and deterministic two-qubit interactions among emitters. A handful of emitters often suffice to generate useful photonic graph states that would otherwise require millions of single photon sources using the linear-optics method. But, photon loss poses an impediment to this method due to the large depth, i.e., age of the oldest photon, of the graph state, given the typically large number of slow and noisy two-qubit CNOT gates required on emitters. We propose an algorithm that can trade the number of emitters with the graph-state depth, while minimizing the number of emitter CNOTs. We apply our algorithm to generating a repeater graph state (RGS) for all-photonic repeaters. We find that our scheme achieves a far superior rate-vs.-distance performance than using the least number of emitters needed to generate the RGS. Yet, our scheme is able to get the same performance as the linear-optics method of generating the RGS where each emitter is used as a single-photon source, but with orders of magnitude fewer emitters.

I. INTRODUCTION

Quantum information processing has the potential to revolutionize cryptography, computation, communications, sensing and imaging. Highly entangled states, called *graph states*, are a key resource for various quantum information applications spanning cryptography, computation [1–4], communications [5, 6] and sensing [7].

Graph states of photonic qubits are being pursued for measurement-based linear optical quantum computation (LOQC), where single photons are used as qubits—often generated using a nonlinear optical process such as heralded spontaneous parametric downconversion (SPDC), whereas gates and measurements are performed using linear optical elements and photon detection. A hindrance to generating photonic graph states using single photons and linear optics is that two-qubit gates and measurements are inherently probabilistic, which makes creating graph states a very resource intensive process [8–10].

Graph states of atomic qubits, such as trapped-ions and color centers, are also of interest. Applications include measurement based quantum computing, quantum repeaters and entanglement assisted sensing [11]. We refer to this genre of matter qubits as *emitters* as they can emit a photonic qubit that is entangled with its internal (e.g., spin) qubit, henceforth referred to as an emitter qubit or simply as an emitter. One way a graph state can be realized among emitters [12, 13] is by entangling emitters pairwise by first having each emitter emit a photon entangled with the respective emitter qubit, and a photonic Bell State Measurement (BSM) performed on

the two photonic qubits using linear optics [14]. Even though the photonic BSM is probabilistic, one can use a ‘shelving qubit’ to which an emitter qubit has arbitrary (deterministic) two-gate gates available, to realize any two-qubit deterministic gate, such as a CNOT gate, between two emitter qubits, deterministically. But such a deterministic CNOT gate between two emitters can take much longer than it takes to perform a single-qubit gate on an emitter, as it relies on repeated probabilistic photonic BSM attempts (See Appendix A for a detailed discussion of how this works and the relevant timescales). Examples of shelving qubits for emitters include: the ²⁹Si nuclear spin qubit for a silicon vacancy in diamond color center where the silicon atom’s electron spin is the emitter qubit [15], and the long-lived optically-inactive ¹⁷¹Yb⁺ ion in the case of a dual-species ion trap where the ¹³⁸Ba⁺ ion is the optically-active emitter qubit [16].

Our work concerns with the problem of preparing a photonic graph state using emitters as a resource. Two naive approaches to this are: (a) first prepare the required graph state on an array of emitters and then transduce the graph state onto photons using single emitter-photon interactions, and (b) use each emitter as a single photon source, followed by (probabilistic) linear optical operations to build up the graph state. In method (a), the number of emitters required is equal to the number of qubits in the photonic graph state, or a constant factor larger if a percolation-based approach is used [13]. In method (b), the number of emitters required is much larger than the number of qubits in the photonic graph state if a deterministic production of the photonic graph state is desired, due to the need of multiplexing to combat the probabilistic linear optical operations. The two properties of emitter qubits we discussed above, are: (1) the ability to deterministically generate photons (possi-

* These authors contributed equally.

bly entangled with the emitter), and (2) deterministic two-qubit gates on a pair of emitters. The naive approaches mentioned above do not effectively leverage the second property. Motivated by getting around the need to have n emitters to prepare an n qubit photonic graph state, Refs. [17, 18] proved an equivalence between D -dimensional matrix product states with open boundary conditions, and states that are generated sequentially and isometrically via a D -dimensional ancillary system which decouples in the last step. This effectively restricts the number of emitters required to generate photonic graph states according to the entanglement property of the graph. They further gave the isometries needed for certain multi-qubit states such as GHZ, W state and graph state. Ref. [19] further explored the generation of 1D-graph states incorporating noise in their generation model. An experimental demonstration of such states was presented in [20, 21]. In Ref. [22], the authors gave a proposal to produce 2-dimensional photonic graph states by leveraging both of the aforesaid properties of emitter qubits. The idea of entangled emitters emitting entangled photons has been exploited in further proposals of generation of photonic graph states in [23–27], for various resource states – such as repeater graph states, one-way quantum computing. [25, 28], allowed for reinterference of photons with emitters after emission. In [29], the authors used matter qubits to produce photonic graph states and analyzed in detail the trade-off between resources and performance, as characterized by the achievable secret key rate per matter qubit. In [30], the authors gave a circuit to generate a general photonic graph state defined by graph G with the minimal number of emitters – as defined by the *height function*, $h(G)$.

While applying CNOT gates on two emitters, leveraged by the aforesaid schemes, is deterministic, the time-scale required to implement a CNOT can be quite large, as discussed earlier. Thus, reducing the circuit depth would be vital. This is because, if we use the minimal number of emitters as quantified in [30] to generate a large photonic graph state, and the application requires the entire graph state to be available for it to work, the oldest photons in the graph state could accrue too much loss for the graph state to be useful for the application.

In this paper, we first expand on the work of [30] to give a method to generate an n -qubit photonic graph state defined by graph G using k emitters, where $k \in [h(G), n]$ can be chosen as needed based on the desired age gap between the oldest and the newest photon in the graph state. We give a circuit decomposition for generating the graph states in terms of Clifford gates and computational basis measurements on emitters. If $k < n$, the photons of the graph state are not released in the same time step. Between the time of release and the time of usage, the photons will undergo loss, introducing noise in the graph state. Our second contribution is an application of our scheme to generating a repeater graph state (RGS) for an all-photonic quantum repeater architecture studied in [10], and an associated resource-performance

tradeoff analysis when our scheme is employed with a chosen number of emitters at each repeater node. We find that if k emitters are used to generate the RGS, the $k = h(G)$ extreme from [30] results in suboptimal performance because of the accumulated photon losses. On the other hand, the other extreme of using each emitter as a single-photon source followed by probabilistic linear optical operations, i.e., the scheme studied in [10], results in requiring a very large number of emitters to obtain a desired rate-versus-distance performance with the repeater architecture. Our scheme can be employed in a way such that even though the number of emitters used at each repeater is larger than $h(G)$, it could still be orders of magnitude smaller than when using each emitter as a single photon source.

II. NOTATION

Consider a graph $G \equiv (V, E)$, where V represents the set of vertices and E represents the set of edges. To define a graph state, we associate each vertex of the graph with a qubit. The graph's edges are associated with the action of controlled-phase (CZ) gates. Mathematically, for a given graph G , the graph state is defined as:

$$|G\rangle = \prod_{i,j \in E} \text{CZ}_{i,j} |+\rangle^{\otimes |V|}, \quad (1)$$

where $\text{CZ}_{i,j}$ represents a CZ gate with vertex i as the control qubit and vertex j as the target qubit. Here, $|+\rangle^{\otimes |V|}$ denotes the initialization of $|V|$ qubits in the $|+\rangle$ state.

Alternatively, a graph state can be described using the stabilizer formalism. For each vertex j , we define an operator $S_j = X_j \prod_{k \in \mathbf{N}(j)} Z_k$, where $\mathbf{N}(j)$ denotes the neighborhood of vertex j in the graph G . Then, the graph state is defined as the simultaneous eigenstate with eigenvalue $+1$ of the operators $\{S_j\}_{j \in V}$.

We note that the graph state can accommodate photonic or matter qubits. We use dual-rail encoding for the photonic qubits. We name the qubits in the graph state as follows: the notation k_p represents photonic qubits, where k is a positive integer. We use the notation j_e to represent emitter qubits, where j is a positive integer.

We utilize the algorithm developed in this work to analyze the properties of repeater graph states [6, 31]. The repeater graph states (RGS) were primarily introduced to give way to an all-photonic quantum repeater architecture. To achieve this Ref. [6] replaced the matter-based quantum memories in [32], by the optical graph states along the lines of [31]. These optical graph states, can be thought of as photonic quantum memories, paving the way for an all photonic repeater architecture. The RGS are then characterized by two parameters m and \bar{b} . Here, m is connected to the multiplexing in the architecture, i.e. m physical qubits are sent to the two nodes on either

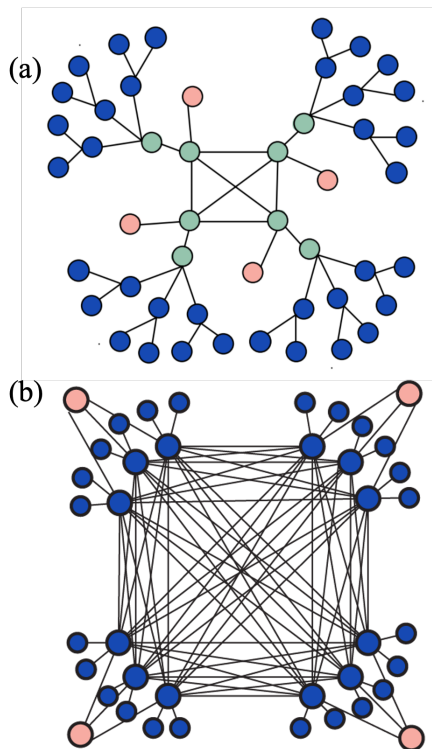


FIG. 1. This figure shows construction of a RGS with $m = 2$, and $\vec{b} = \{3, 2\}$. (a) Start with a clique graph state with $2m$ qubits. Attach a qubit (pink qubits) and a tree with branching vector \vec{b} to every qubit of the clique graph state. (b) Performing X measurements on the green nodes on the graph state in (a) gives the RGS. The pink qubits depict the flying qubits, which are sent to the two adjacent nodes, and the dark blue nodes remain at the repeaters and mimic quantum memories.

side of the repeaters. The physical qubit is loss-error protected by a regular tree described by the branching vector $\vec{b} \equiv \{b_0, b_1, \dots, b_d\}$, which signifies that the root of the tree has b_0 children nodes, and each of those nodes have b_1 children nodes, till we reach the $(d + 1)^{\text{th}}$ level. An illustrative example is depicted in FIG. 1.

III. OVERVIEW AND MAIN RESULTS

We are given a graph state $|G\rangle$ and n quantum emitters. Each quantum emitter can emit photons. The emission process can be modeled as a CNOT gate. The emission process modelled as the CNOT gate is the only allowed interaction between the emitters and the photons. We also have access to the following operations: arbitrary single-qubit (including Pauli, Hadamard and non-Clifford) gates on both the emitter and the photon qubits, CNOT gates between two emitters, and single-qubit measurement of the photonic and the emitter qubits. We note here that the application of CNOT gates between emitters, while deterministic, is hard to

implement (see Appendix A).

We now pose the following question:

Given n emitters and a desired (photonic) graph state $|G\rangle$, what is the algorithm to generate the graph state using the emitters, keeping in mind the restrictions in the architecture delineated above?

The optimality of the algorithm is highly dependent on the objective function. One could in principle, seek to minimize the circuit depth for CNOT gates, minimize the number of CNOT gates used in the circuit, or minimize the number of emitters as done in [30]. One could also anticipate an application-based objective function.

Graph state generation is also challenging due to the limited architecture of the platform, which prohibits any further interactions between the emitted photons and emitters. All entanglement in the graph state must be created solely by the CNOT gates modeling the emitters and the photon emission process. Consequently, the sequence in which the photons are released needs to be carefully designed. Additionally, the time required to emit photons is significantly shorter than the time needed to implement CNOT gates between the emitters. Therefore, it is crucial to parallelize and minimize the application of CNOT gates.

In this work, we do not consider an optimal objective function, but rather give an algorithm which can generate the graph state keeping in mind the limitations of the platform. We then give an algorithm to calculate the CNOT depth and give the time at which each photon in the graph state is generated accounting for realistic time frames of Clifford gates, measurements, CNOT gates and emission processes. We refer to the time at which a photon is emitted as its *emission time*. We take the emission time of the first emitter photon as a reference point and calculate the emission times of the remaining photons accordingly. The emission times are a function of the implementation times of Clifford gates, measurements, and CNOT gates.

Our algorithm draws inspiration from a previous work [30]. First, we use time-reversed sequences from [30], which means that given a graph state, we obtain the circuit that converts the graph state to a product state. In this time-reversed context, the photon emission is replaced with (a hypothetical) photon absorption. By time-reversing the sequence, we obtain an emission sequence that returns the product state to the target state. The task of reversing quantum gates is straightforward except for measurements. To this end, we borrow the time-reversed measurement technique introduced in [30].

To convert any graph state to a product state, it is sufficient to apply CNOT gates between the qubits connected by the edges. The main challenge is that two-qubit gates are unavailable between photons. Therefore, the removal of entanglement needs to be mediated by the photon absorption process or CNOT gates between emitters. Our algorithm works as follows: we swap the

emitters and photons using time-reversed measurements. Then, we remove entanglement through the photon absorption process and two-qubit CNOT gates. That is, we can eliminate the edges in two ways: via the photon absorption process or the application of CNOT gates between emitters. However, the time required for these two processes differs significantly, with photon absorption/emission being more favorable in current experimental platforms. Consequently, we prioritize removing entanglement through the absorption process whenever possible in lieu of applying CNOT gates between emitters.

Our second contribution is the application of our method to the performance evaluation in the context of all-photonic quantum repeater chain using the standard RGS method [10]. We compare the resource requirements of the following three methods for each repeater node to prepare the RGS:

1. Method 1 uses the least, i.e., $h(G)$ number of emitters,
2. Method 2 uses each emitter as a single photon source, and probabilistic stitching of the photons into the RGS, and
3. Method 3, our method, where we can increase the number of emitters used (above $h(G)$), to trade with lowering the resulting circuit depth (and hence reducing the photon loss and the number of emitter CNOTs).

We compare the three schemes in terms of the number of emitters required per repeater node to obtain a desired rate-versus-distance performance.

We observe that:

- In general, in the context of our method (3) above, increasing the number of emitters used to generate the RGS improves the rate-vs.-distance performance,
- For an assumed parameter regime of a generic emitter system, we show that our scheme's emitter-array size and CNOT-depth can be calibrated such that under identical loss conditions, our scheme (3) is able to achieve the same performance as the linear-optics method (2) [10], but with orders of magnitude fewer emitters,
- Using the method (1) of using the least-possible number of emitters [24] performs worse than the other two methods, given the extreme losses incurred by the photons in the generated RGS.

IV. ALGORITHMIC BUILDING BLOCKS

Given a graph state $|G\rangle$ with m photonic qubits and n emitters prepared in state $|0\rangle^{\otimes n}$. Taking inspiration

from [30], the goal of our algorithm is to convert the graph state and emitters into $|0\rangle^{\otimes n+m}$. We begin by introducing the three primitives used in our algorithm:

- **Swapping by the free emitter (SFE)** - Absorb a photon when the emitter is in the (unentangled) state $|0\rangle$.
- **Photon absorption** - Absorb a photon when the emitter is entangled with photonic qubits in $|G\rangle$ under certain condition explained in Section IV B.
- **Emitter interaction** - Remove the edges between the emitter nodes.

We then combine the three primitives to yield the final algorithm.

A. Swapping by the free emitter

Let $|G\rangle$ be an arbitrary graph state consisting of photonic and emitter qubits. If an emitter k_e is in the $|0\rangle_{k_e}$ state – called a free emitter, we give a circuit to implement the following action:

$$\text{SWAP}_{j_p \leftrightarrow k_e} |G\rangle \otimes |0\rangle_{k_e}, \quad (2)$$

where $\text{SWAP}_{j_p \leftrightarrow k_e}$ corresponds to swapping the photonic qubit j_p in $|G\rangle$ with the emitter qubit k_e , $j \in [1, m]$ and m is the total number of qubits in the graph state. This action replaces the j_p qubit in the vertex set V of the graph G by the k_e qubit.

The circuit given in FIG. 2(a) implements this above action. In a state of the form $|G\rangle \otimes |0\rangle_{k_e}$, the k_e qubit does not share any edge with the graph state $|G\rangle$. The stabilizer generator associated with this state can be expressed as the left-hand corner of Eq 3. P_j represents a Pauli acting on the j^{th} qubit, and $P_{V \setminus \{j_p\}}, \tilde{P}_{V \setminus \{j_p\}}$ denote the tensor product of Pauli operators acting on all vertexes of the graph except j_p . The Hadamard and CNOT $_{c,t}$ operations transform the stabilizers as follows [33]:

$$\begin{array}{cc} X \xrightarrow{H} Z & Z \xrightarrow{H} X \\ X_c I_t \xrightarrow{\text{CNOT}_{c,t}} X_c X_t & I_c X_t \xrightarrow{\text{CNOT}_{c,t}} I_c X_t \\ Z_c I_t \xrightarrow{\text{CNOT}_{c,t}} Z_c I_t & I_c Z_t \xrightarrow{\text{CNOT}_{c,t}} Z_c Z_t \end{array}$$

We then express the action of the circuit given in Figure 2(a) on the stabilizer generator.

$$\begin{array}{ccc} P_{V \setminus \{j_p\}} & Z_{j_p} & I_{k_e} \\ \tilde{P}_{V \setminus \{j_p\}} & X_{j_p} & I_{k_e} \\ I_{V \setminus \{j_p\}} & I_{j_p} & Z_{k_e} \end{array} \xrightarrow{H_{k_e}} \begin{array}{ccc} P_{V \setminus \{j_p\}} & Z_{j_p} & I_{k_e} \\ \tilde{P}_{V \setminus \{j_p\}} & X_{j_p} & I_{k_e} \\ I_{V \setminus \{j_p\}} & I_{j_p} & X_{k_e} \end{array} \xrightarrow{\text{CNOT}_{k_e, j_p}} \begin{array}{ccc} P_{V \setminus \{j_p\}} & Z_{j_p} & Z_{k_e} \\ \tilde{P}_{V \setminus \{j_p\}} & X_{j_p} & I_{k_e} \\ I_{V \setminus \{j_p\}} & X_{j_p} & X_{k_e} \end{array} \xrightarrow{H_{k_e} \otimes H_{j_p}} \begin{array}{ccc} P_{V \setminus \{j_p\}} & X_{j_p} & X_{k_e} \\ \tilde{P}_{V \setminus \{j_p\}} & Z_{j_p} & I_{k_e} \\ I_{V \setminus \{j_p\}} & Z_{j_p} & Z_{k_e} \end{array} \xrightarrow{\text{CNOT}_{k_e, j_p}} \begin{array}{ccc} P_{V \setminus \{j_p\}} & I_{j_p} & X_{k_e} \\ \tilde{P}_{V \setminus \{j_p\}} & Z_{j_p} & Z_{k_e} \\ I_{V \setminus \{j_p\}} & Z_{j_p} & I_{k_e} \end{array} \xrightarrow{I_{j_p} \otimes H_{k_e}} \begin{array}{ccc} P_{V \setminus \{j_p\}} & I_{j_p} & Z_{k_e} \\ \tilde{P}_{V \setminus \{j_p\}} & I_{j_p} & X_{k_e} \\ I_{V \setminus \{j_p\}} & Z_{j_p} & I_{k_e} \end{array} \quad (3)$$

The final stabilizer is equivalent to applying the swap gate on j_p qubit of the graph state $|G\rangle$ and qubit k_e associated with the free emitter.

The time-reversed implementation of Eq 3 is given in FIG. 2(b). The first CNOT gate, corresponds to the emitter emitting the photon. To implement the second CNOT gate, we would require an interaction between the photon and the emitter after the photon has been emitted. However, this interaction is not allowed according to the architecture constraints. FIG. 2(c) shows an equivalent implementation of the circuit given in FIG. 2(b). To observe this, note that after the completion of the circuit in FIG. 2(b), the emitter is in the $|0\rangle_{k_e}$ state. This constraint allows us to model the $CNOT_{k_e, j_p} \otimes H_{k_e}$ by a computation measurement on the emitter followed by a controlled X rotation on the photon. That is, if the emitter measurement outcome is one, then apply a Pauli X on the photon. The Pauli-X gate on the photonic qubit affects only the phase of the stabilizer of $|G\rangle$. As a result, it is not necessary to physically apply the Pauli-X gate if we keep track of the phase of the stabilizers using classical post-processing. We call this primitive the swapping by the free emitter (SFE). This implementation is similar to the time-reversed measurement introduced in [30].

To implement this primitive, we need to specify the qubit in the graph that the emitter needs to replace. This specification is given to the algorithm under the initial conditions. Finding the optimal initial conditions are beyond the scope of this work.

The impact of the replacement by the free emitter on the graph can be represented pictorially as well, as given in FIG. 3.

B. Photon absorption

Next, we delineate the conditions under which an emitter can absorb a photon. For each case, we write the initial and final stabilizer and pictorially give the impact of the absorption on the graph state.

1. Case 1

Let $|G\rangle$ be an arbitrary graph state consisting of photonic and emitter qubits. Consider $k_e, j_p \in V(G)$, and $\mathbf{N}(k_e) = \{j_p\}$. That is, the neighborhood of the emitter qubit k_e consists of just a photonic qubit j_p . Then, we apply a Hadamard gate on k_e followed by $CNOT_{k_e, j_p}$. The $CNOT_{k_e, j_p}$ gate is equivalent to the absorption of the j_p photon by the k_e emitter. The transformed graph is denoted by G_1 . The aforementioned action performs the following transformation on the stabilizer generator:

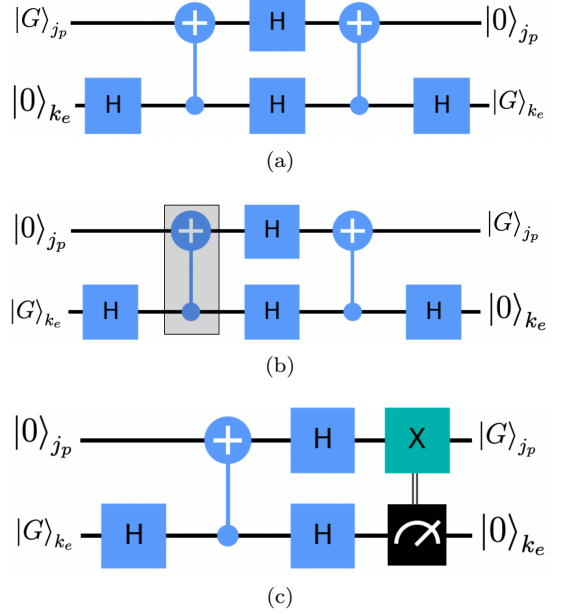


FIG. 2. Time reversed circuit for swapping of photon in the graph state by a free emitter. $|G\rangle_{k_e}$ corresponds to the k_e emitter in the graph state $|G\rangle$ and $|G\rangle_{j_p}$ corresponds to the j_p photon in the graph state $|G\rangle$. (a) Circuit for implementation of Eq 2 (b) Time-reverse circuit for FIG. 2(a). The shaded CNOT corresponds to the emission process. (c) Platform compatible implementation of Eq 2.

$$\begin{array}{ccc}
 \begin{array}{l} I_{V \setminus \{j_p, k_e\}} \\ P_{V \setminus \{j_p, k_e\}} \\ \tilde{P}_{V \setminus \{j_p, k_e\}} \end{array} & \begin{array}{l} X_{k_e} \\ Z_{k_e} \\ I_{k_e} \end{array} & \begin{array}{l} Z_{j_p} \\ X_{j_p} \\ Z_{j_p} \end{array} \\
 & & \xrightarrow{H_{k_e}} \\
 \begin{array}{l} I_{V \setminus \{j_p, k_e\}} \\ P_{V \setminus \{j_p, k_e\}} \\ \tilde{P}_{V \setminus \{j_p, k_e\}} \end{array} & \begin{array}{l} Z_{k_e} \\ X_{k_e} \\ Z_{k_e} \end{array} & \begin{array}{l} Z_{j_p} \\ X_{j_p} \\ Z_{j_p} \end{array} \\
 & & \xrightarrow{CNOT_{k_e, j_p}} \\
 \begin{array}{l} I_{V \setminus \{j_p, k_e\}} \\ P_{V \setminus \{j_p, k_e\}} \\ \tilde{P}_{V \setminus \{j_p, k_e\}} \end{array} & \begin{array}{l} I_{k_e} \\ X_{k_e} \\ Z_{k_e} \end{array} & \begin{array}{l} Z_{j_p} \\ I_{j_p} \\ I_{j_p} \end{array}
 \end{array} \quad (4)$$

Note that the emitter k_e has an edge only with the j_p , while the j_p qubit shares an edge with the k_e emitter and possibly other qubits in the graphs. Then, each stabilizer in the generator would have the form given on the left-hand side of the Eq 4.

Let $E^G(i)$ be the set of edges incident on vertex i of the graph G . Then for the graph G_1 , $E^{G_1}(k_e) = E^G(j_p) \setminus \{(k_e, j_p)\}$, where j_p refers to the j^{th} photon in the graph state and k_e refers to the k^{th} quantum emitter. The stabilizer representation of the final graph state $|G_1\rangle$ implies that the j_p photon is in the state $|0\rangle$, the edge between k_e and j_p has been removed, and the remaining edges of j_p have been transferred to k_e . That is, $E^{G_1}(k_e) = E^G(j_p) \setminus \{(k_e, j_p)\}$. For a pictorial representation of the transformation of the graph state, see FIG. 4.

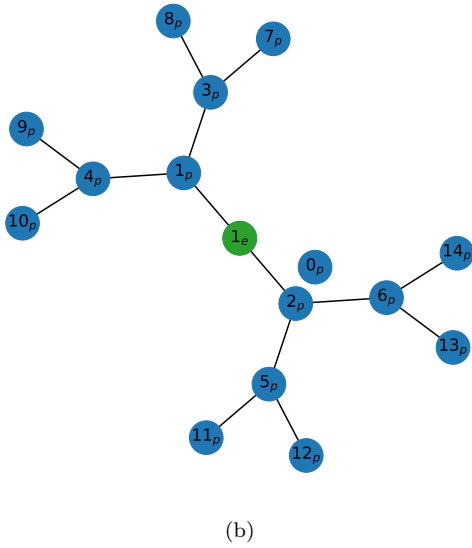
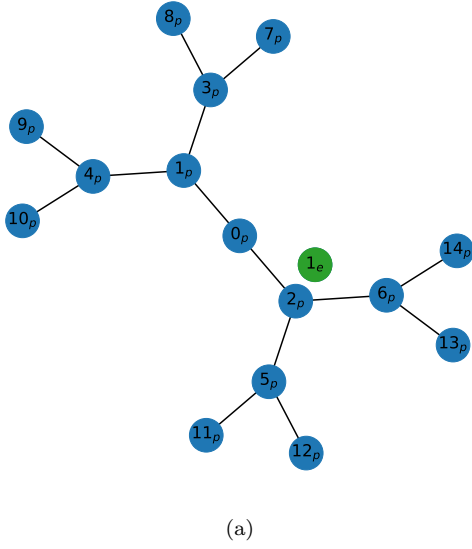


FIG. 3. Pictorial representation of swapping of photon by an emitter (a) State before SFE (b) State after the implementation of SFE

2. Case 2

Let $|G\rangle$ be an arbitrary graph state consisting of photonic and emitter qubits. Let $j_p, k_e \in V(G)$ and let $\mathbf{N}(j_p) = \{k_e\}$. Then, we apply a Hadamard gate on j_p and a CNOT_{k_e, j_p} gate. The aforementioned action performs the following transformation on the stabilizer group.

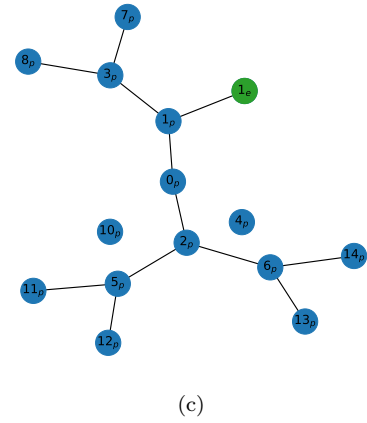
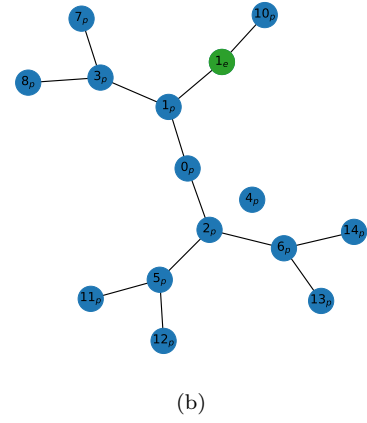
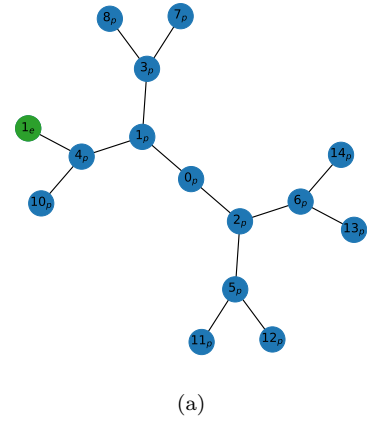


FIG. 4. Pictorial representation of photon absorption (a) Initial state for case 1 (b) Final state for case 1, initial state for case 2 (c) Final state for case 2

V. FINAL ALGORITHM

We combine the three primitives outlined in Section IV A, IV B, IV C to obtain the final algorithms. We note here that, in principle, a variety of ways exist to combine the above primitives to absorb the graph state completely. Our numerics show that with the objective to minimize the CNOT depth of the circuit for repeater graph states, the following two algorithms yield the minimal CNOT depth. The choice of the algorithm depends on the initial number of emitters. Further optimization on the ordering of the primitives is left for future work.

Both the algorithms take as input the number of emitters, the initial condition, and the graph state. The initial condition gives the preferred order for choosing photons for SFE. Recall that for the SFE, we have to specify which photon the free emitter should absorb. This specification is given by the initial conditions – an ordered list of photons in the graph state.

The goal of the algorithm is to convert the graph state $|G\rangle$ with m photon qubits and n emitters prepared in the state $|0\rangle^{\otimes n}$ to $|0\rangle^{\otimes n+m}$. The output of the algorithm is the sequence of operations that achieve the goal. We can then time reverse the output to obtain the sequence of operations which starting from $|0\rangle^{\otimes n+m}$ gives a state $|G\rangle \otimes |0\rangle^{\otimes m}$.

A. Algorithm 1

1. Absorb as many photons as possible via the quantum emitters using the steps outlined in IV B. If no more photons can be absorbed, move to Step 2. If no quantum emitter exists in the graph state, move to Step 2. Remove the absorbed photons from the initial condition.
2. Use the primitive of SFE given in Section IV A to swap a photon with a free emitter. The initial conditions give the photon to be swapped. Remove the swapped photon from the initial condition. Repeat 1. If no more free emitters exist, move to Step 3.
3. Perform the steps laid out in Section IV C to remove entanglement between the emitters.
4. Repeat steps 1-4 till all photons have been absorbed.

In Algorithm 1, we repeatedly remove the absorbed photons from the initial conditions. The reason being that once the photon has been absorbed, it cannot be swapped with a free emitter. If the number of emitters entered into the algorithm is insufficient, then not all photons will be absorbed.

We also note that with this algorithm, there is an upper limit on the number of emitters that can be used. This algorithm gives a preference to photon absorption over SFE. This implies that the emitter absorbs as many

photons as possible. Then, after a point, there are no more photons left for the emitter to replace. To incorporate more emitters, we would need a different ordering of the primitives, as depicted in Algorithm 2. The Algorithm 2 gives preference to replacing the photons with quantum emitters over photon absorption.

B. Algorithm 2

1. Absorb as many photons as possible via the quantum emitters using the steps outlined in Section IV B. If no more photons can be absorbed, move to Step 2. If no quantum emitter exists in the graph state, move to Step 2. Remove the absorbed photons from the initial condition.
2. Use the primitive of SFE given in Section IV A to swap photons by all possible free emitters. The initial conditions give the photons to be swapped. Remove the swapped photons from the initial condition.
3. Absorb as many photons as possible via the quantum emitters using the steps outlined in Section IV B. If no more photons can be absorbed, move to Step 4. Remove the absorbed photons from the initial condition.
4. Perform the steps laid out in Section IV C to remove entanglement between the emitters.
5. Repeat Steps 1-4 till all photons are absorbed.

The main point of difference between Algorithm 1 and Algorithm 2 is as follows: In Algorithm 1, after swapping the photon with an emitter, the emitter tries to absorb as many photons as possible. The algorithm tries to swap another photon with a free emitter if no more photons can be absorbed by the existing emitters in the graph. The Algorithm 1 prefers absorbing photons over swapping with free emitter. In Algorithm 2, the preference is given to swapping photons with free emitters. The Algorithm will first swap photons with all available free emitters and then try to absorb photons.

Now, consider that the number of emitters equals the number of photons in the graph state. Then, the Algorithm 2, first prepares the graph state on the emitter and transduces the state to the photons. In this case, all the photons are emitted in one time step.

C. Example for Algorithm 1

We illustrate Algorithm 1 with the following example. Two parameters m and the branching vector \vec{b} describe a repeater graph state. For this example, we choose $m = 2$ and $\vec{b} = \{3, 2\}$. We choose the number of emitters as twelve. The initial conditions are given as a list of the

end nodes of the attached tree, implying that the emitters can replace these photons if the other emitters have not absorbed them.

The initial graph state is given in FIG. 7(a). The emitter 1_e replaces 10_p via SFE to yield the graph in FIG. 7(b). The $\mathbf{N}(1_e) = 7_p$, then the emitter 1_e can absorb 7_p to yield FIG. 7(c). The $\mathbf{N}(11_p) = 1_e$, then the emitter 1_e can absorb 11_p to yield FIG. 7(d). Next, $\mathbf{N}(1_e) = 6_p$, implying that the emitter 1_e can absorb 6_p to obtain the graph in FIG. 7(e). We next see that the emitter 1_e can absorb no further. At this point, we use the initial conditions, and the emitter 2_e replace the photon 12_p . We can then, by looking the photon absorption criterion given above, see that the emitter 2_e can absorb 8_p and 13_p to yield the graph given in FIG. 7(g). Now, the emitter $1_e, 2_e$ can absorb no further photons. The emitter 3_e replaces the 14_p photons and absorbs 9_p and 15_p photons to yield the graph given in FIG. 7(h). In this manner, we use the 12 emitters to start by absorbing at the end nodes. This gives us the graph in FIG. 7(i). Next, we no longer have any free emitters available, and we start with emitter disentanglement. All the edges between the emitters are removed by the application of CNOT gates between quantum emitters to yield the graph given in FIG. 7(j). The absorption process continues until all the photons have been absorbed to yield the graph in FIG. 7(o). Then, the emitters are disentangled to yield a completely unentangled state.

D. Circuit depth

In both the algorithms presented above, only in the emitter disentanglement step, we apply CNOTs between quantum emitters. The $\text{CNOT}_{e,e}$ is the most time-consuming resource that we have in this architecture. To this end, we seek to calculate the circuit depth in terms of $\text{CNOT}_{e,e}$.

In the algorithm specified above, the application sequence of $\text{CNOT}_{e,e}$ s is not fixed in the emitter disentanglement step. In principle, we would like to parallelize the $\text{CNOT}_{e,e}$ s in order to reduce the depth. This work uses the following algorithm to calculate the depth without claiming optimality. We are given the list of $\text{CNOT}_{e,e}$ s applied during the emitter disentanglement step. The $\text{CNOT}_{e,e}$ s in this list can be applied in any sequence.

For each emitter disentanglement step, the algorithm is as follows:

1. From the list of $\text{CNOT}_{e,e}$ s, choose CNOTs that act on independent emitters. These CNOTs can be applied in one-time step or in parallel.
2. Remove the chosen CNOTs from the list of applied $\text{CNOT}_{e,e}$ s.
3. Repeat steps 1-2 till no CNOTs are left in the list of applied $\text{CNOT}_{e,e}$ s.

4. The number of repetitions gives the CNOT depth for the emitter disentanglement circuit.

Then, the sum of the CNOT circuit depth for each emitter disentanglement step gives us the CNOT circuit depth of the entire state generation circuit.

Note that in the above algorithm, in the first step, there are multiple ways to choose between the independent CNOTs. We do not optimize for this choice of CNOTs.

1. Example: Calculation for CNOT Depth

FIG. 8, shows the CNOT depth vs. the number of emitters for various repeater graph states. Note that, in general, an increase in the number of emitters does not imply a decrease in the CNOT depth. For example, one can generate a n -qubit GHZ state with a single emitter, making the circuit's CNOT depth zero. However, when given n -qubits, we can first prepare the graph state on the quantum emitters, transfer the state to the photons and then measure the emitters, also called as transducing the state of emitters on the photons. The CNOT depth of the circuit is two. For FIG. 8, we only use the extra emitter if this decreases the CNOT depth.

We see here the impact of the objective function on the choice of algorithm. If the goal is to reduce the time difference between the generation of the initial photons and final photons, then the transducing would be preferable. However, if the goal is reduce the CNOT depth, then sequential emission is preferable.

VI. EMISSION TIMES OF PHOTONS

To the algorithm given in Section V, we can associate a circuit composed of the following gate-set:

- Hadamard gate on the emitter (H_e). Time required to perform $H_e - t_{H_e}$.
- CNOT gate with the emitter as the control and the photonic qubit as the target ($\text{CNOT}_{e,p}$). Time required - $t_{\text{CNOT}_{e,p}}$. This gate models the emission of the photon.
- CNOT gate between two emitters ($\text{CNOT}_{e,e}$). Time required $t_{\text{CNOT}_{e,e}}$.
- Measuring an emitter in the computational basis. Time taken t_{meas} .
- While not a part of gate set, after each measurement, we need to initialize the emitter in the $|0\rangle$ state. Time required - t_{init} .

We evaluate these timescales for SiV in Appendix A. We also outline the procedure for calculating the emission time of each photon in the graph state in Appendix B.

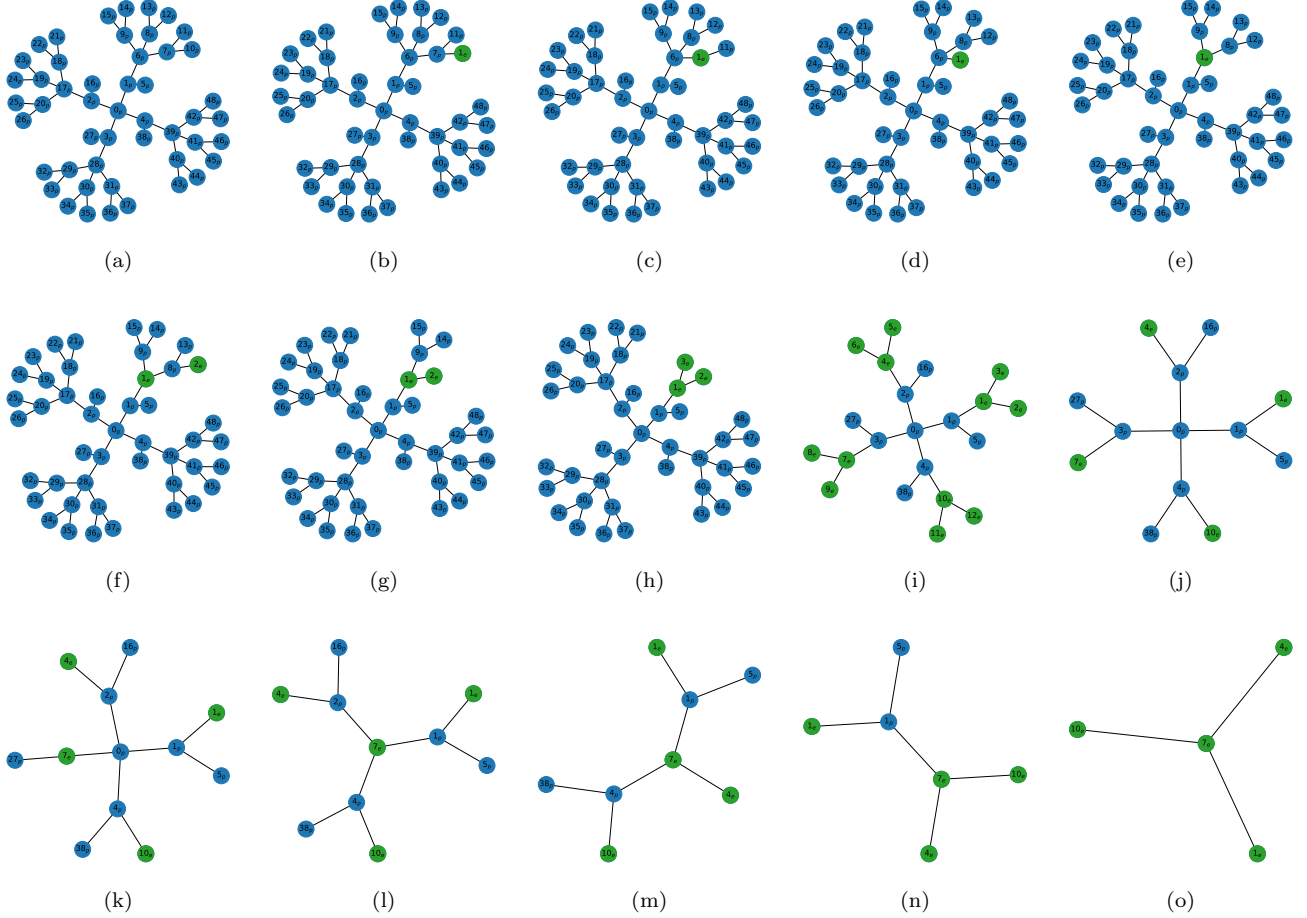


FIG. 7. In this figure, we show the progression of the graph state as the available emitters absorb the photons. The initial state is given in (a).

This information is useful in modeling the losses on the photons before they can be used for the desired application, as shown in Section VII C.

VII. ALL-PHOTONIC QUANTUM REPEATER ARCHITECTURE

One of the primary applications of photonic graph states is as the resource state for the all-photonic quantum repeaters. Each repeater in this architecture is equipped with photonic dual-rail graph states. Each qubit of the graph state is a logical qubit encoded in a tree code [6, 10, 34]. In dual-rail photonic encoding, photon loss results in qubit loss error. The tree code protects the qubits of the graph state from losses, mimicking a quantum memory. Entanglement distribution rates and the maximum key rates over a lossy bosonic channel such as an optical fiber or free space link are known to drop exponentially with loss [35]. The all-photonic quantum repeater architecture with tree-encoded graph state (referred to as repeater graph state

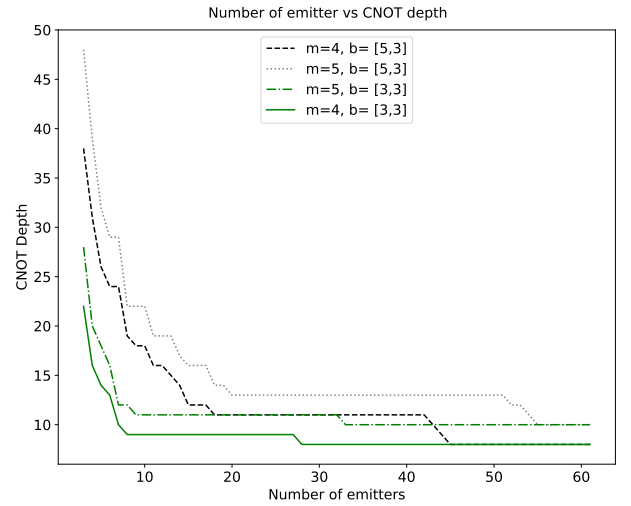


FIG. 8. Emitter vs CNOT depth

(RGS) onwards) outperforms the maximum key rate obtained without using repeaters or the repeaterless rate given by $R_{\text{direct}} = -\log_2(1 - \eta)$ [36], (see also [37] for a strong converse bound). Here, η is the transmissivity of the optical fiber and is proportional to the length of the fiber, L and its loss coefficient α ($\eta = e^{(-\alpha L)}$).

In [10], first, single photons are generated using emitters. Then, they are entangled using linear optical Bell state measurements (BSMs) that are probabilistic and multiplexed to create the RGS. The probabilistic entangling operation results in a massive overhead in the number of emitters required to produce one copy of the RGS. This section compares the performance of the RGS, created deterministically using our algorithm, with the RGS generated using probabilistic BSMs and multiplexing (hereafter referred to as the multiplexing method) in terms of (1) entanglement generation rate and (2) the number of emitters used per repeater.

A. The protocol

We begin by reviewing the all-photonic quantum repeater protocol. FIG. 9(b) shows a chain of n all-photonic quantum repeaters placed equidistant between the users Alice and Bob with m parallel optical channels connecting each pair of repeaters. We refer to m as the degree of multiplexing. In an all-photonic quantum repeater protocol, once the repeater graph state (RGS) (see FIG. 9(a)) is generated at every repeater, the grey qubits or the *link* qubits from the RGS are sent over the optical channels. The link qubits from the neighboring repeaters meet at the minor nodes, placed halfway between the neighboring repeaters, and undergo a photonic Bell state measurement (BSM). This measurement succeeds with probability p . If the users are placed distance L apart, $p = \eta^{1/(n+1)} p_{\text{BSM}}$, where p_{BSM} is the success probability of the linear optical BSM and $\eta = \exp(-\alpha L)$. In other words, the BSM at the minor nodes succeeds if both the qubits undergoing BSM reach the minor node and the BSM itself is successful. For a simple linear optical system, $p_{\text{BSM}} = 50\%$, which can be boosted using ancilla single photons. If a BSM between the link qubits is successful, we say a *link* was established. The success or failure outcomes of the BSMs are classically communicated to the respective neighboring repeaters.

Once the repeaters receive the classical communication regarding the BSM outcomes, every repeater performs X measurements on a pair of logical qubits with successfully heralded links on the opposite sides of the repeater and Z measurements on the remaining $2m - 2$ logical qubits in the graph state. These measurements are probabilistic as they are performed on lossy photonic qubits. If all measurements at every repeater are successful and at least one BSM succeeds at every minor node, users Alice and Bob end up with a shared Bell state. The entanglement

generation rate is given by [10]

$$R = \frac{P_X^{2n} P_Z^{2(m-1)n} [1 - (1-p)^m]^{(n+1)}}{2m\tau} \text{ebits/s} \quad (7)$$

Here, P_X and P_Z are the probabilities of success of the logical single qubit X and Z measurements at the repeaters, respectively, and τ is the repetition time of the protocol. Eq. 7 assumes that qubits in all repeaters have identical P_X and P_Z . The success probabilities of the Pauli measurements depend upon the shape and the size of the tree code used as we discuss in the following section.

B. Tree code

In this section, we derive the success probabilities of Pauli measurements on the logical qubit of a tree code assuming the qubits in the tree code have non-uniform loss probabilities. As discussed in Section II, we define a tree graph state using branching vector $\vec{b} \equiv \{b_0, b_1, \dots, b_d\}$. We define the root (labeled as qubit 0) of the tree as the qubit on level 0 of the tree as shown in FIG. 10(a). Let l_i be the probability of loss of qubit i of the tree and $\mathcal{C}(i)$ be the set of *children* of i , i.e., the qubits one level below i . Similarly, i is the *parent* of qubits in $\mathcal{C}(i)$. In order to encode a physical qubit into a tree code, a tree graph state is first attached to the physical qubit using a CZ gate as shown in FIG. 10(b). X measurements on the tree's root and the physical qubit encode the physical qubit into the logical qubit.

The tree code protects the logical qubit from loss using the *counterfactual* error correction scheme [34]. This scheme aims to infer a Pauli measurement result in the event a qubit of a graph state is lost by performing measurements on the other qubits in the graph state. For example, consider a graph state stabilizer $Z_i X_j \prod_{k \in \mathcal{C}(j)} Z_k$. If the Pauli operators in this stabilizer are measured, the product of all measurement outcomes is 1. Using this property, if qubit i is lost, the Z measurement outcome of i can be inferred from the outcomes of X measurement on j and Z measurements on the set of qubits in $\mathcal{C}(j)$. This is an *indirect-Z* measurement. Note that, direct- Z measurement succeeds if the qubit is not lost. For qubit i , the probability of success of direct or indirect- Z measurement is given by [6, 10],

$$P_{Z_i} = (1 - l_i) + l_i \xi_i \quad (8)$$

Here, ξ_i is the success probability of indirect- Z measurement. We perform indirect- Z measurement on a qubit i in a tree graph state using stabilizers of the form $Z_i X_j \prod_{k \in \mathcal{C}(j)} Z_k$, $j \in \mathcal{C}(i)$. Out of the $|\mathcal{C}(i)|$ possible attempts of an indirect- Z measurement on i , at least one must succeed. The success probability of an attempt is $(1 - l_j) \prod_{k \in \mathcal{C}(j)} P_{Z_k}$. Here, $(1 - l_j)$ is the success probability of X measurement on j . If i is not on the $(d+1)^{\text{th}}$

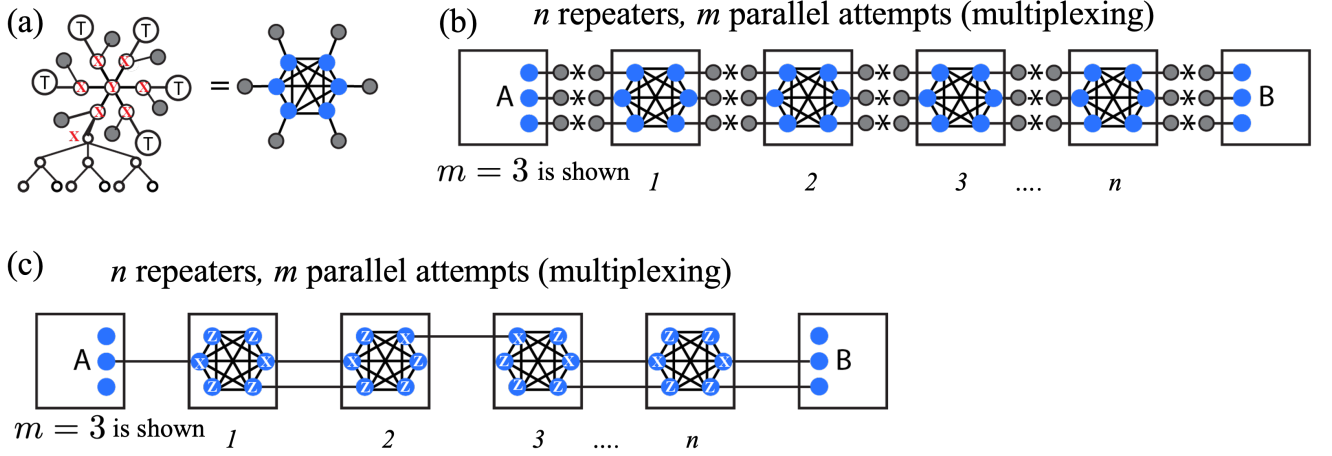


FIG. 9. All-photonic quantum repeater architecture (a) The repeater graph state with tree encoded logical qubits (blue circles) and link qubits (grey circles) (b) A chain of n repeater with multiplexing $m = 3$, placed between the users - A and B. The link qubits are sent over the optical channel and they meet at the minor nodes (denoted by 'x') to undergo a linear optical BSM (c) The solid black lines showing links generated from the successful BSMs at the minor nodes.

(last) level of the tree, using recursion, we can write:

$$\xi_i = 1 - \prod_{j \in \mathcal{C}(i)} \left[1 - (1 - l_j) \prod_{k \in \mathcal{C}(j)} P_{Z_k} \right] \quad (9)$$

We set $\xi_i = 0$ if i is on the $(d + 1)^{\text{th}}$ level of the tree, as i does not have any children, and indirect- Z measurement cannot be performed without children.

The probabilities of successful logical Z and X measurements are [6, 10],

$$P_Z = \prod_{i \text{ on level } 1} P_{Z_i} \quad (10)$$

$$P_X = \xi_0 \quad (11)$$

i.e., the Z measurement probability of the logical qubit is the product of Z measurement probabilities on all the level 1 qubits and the X measurement probability of the logical qubit is the indirect- Z measurement probability on the root qubit.

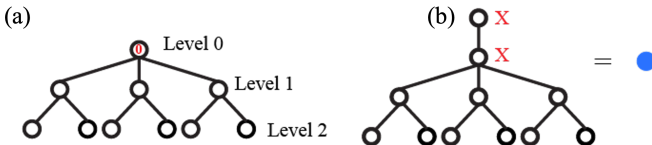


FIG. 10. Tree code (a) Tree graph state with node 0 as the root and the branching vector $\vec{b} = \{3, 2\}$. (b) A logical qubit encoded in a tree code (shown as a blue circle) is created by first attaching the qubit to be encoded to a tree graph state using CZ gate, followed by X measurements on the qubit to be encoded and the root of the tree.

This paper considers tree code with a branching vector of length two. The following section discusses an all-photonic quantum repeater architecture with RGSs generated using the algorithm described in Section V.

C. Emitter-based repeater architecture

As the entanglement rate is inversely proportional to qubit loss, designing a repeater architecture that reduces the losses becomes essential. When quantum emitters are used as single photon sources, the multiplexing method generates the RGS in time t_{init} , in the limit that initializing emitters is much slower than the photonic chip that performs linear optical operations. The entire RGS is created in the same time step, resulting in identical loss probability for every qubit. The emitter-based method emits qubits of the RGS at different times. This section discusses the photonic qubit measurement sequence on the RGS that minimizes the loss and calculates the loss probability of the RGS's qubits for the emitter-based method. It also derives the number of emitters required for the emitter-based method to attain a given repetition time.

1. Photonic qubit measurement sequence

In an all-photonic architecture, the photon loss probability is directly proportional to the lifetime of the photon, i.e., the time between photon generation and measurement. In this section, we outline some properties of the generation scheme that help mitigate the photon loss. Consider a quantum circuit to generate a graph state using two emitters as shown in FIG. 11(b). From

Section IV, Hadamard, Pauli- X , and identity are the only operations performed on the photonic qubits of any graph state after they are emitted. In FIG. 11(b), the photonic qubits are measured in the Pauli basis after generating the entire graph state. Since the measurements commute with operations on other qubits commute, the order of the measurements does not matter. FIG. 11(c) shows an equivalent quantum circuit, s.t. the photonic qubits are measured as soon as the emitter emits the photons. We eliminate the conditional Pauli- X gate as it only affects the phase of the generated state, which can be tracked using classical post-processing. Moreover, we rotate the measurement bases of the photonic qubits instead of performing the Hadamard gates.

Note that we have assumed above that the measurement bases of all qubits are pre-decided. If the measurements are adaptive, i.e., the measurement basis of a qubit depends upon the measurement outcome of another qubit, we must modify the measurement sequence accordingly. For example, consider qubits 2 and 4 from FIG. 11(a) such that the measurement outcome of qubit 2 determines the measurement basis of qubit 4. In this case, we would have to measure qubit 4 after qubit 2, even if it is emitted earlier. This increases the loss probability of qubit 4. Consequently, an all-photonic repeater with fewer adaptive measurements performs better. In the following section, we outline the measurement sequence on the emitted RGS and calculate the loss introduced on each photon.

2. Loss calculations

At the beginning of our protocol, the quantum emitters in all repeaters simultaneously start generating the RGS. The repeaters send link qubits to the minor nodes as soon as they are emitted. Let $\tau_l = L/(2c_f(n+1))$ be the time for the link qubits to reach the minor nodes. Here, c_f is the speed of light in the optical fiber, and L is the distance between the end nodes. Each minor node performs BSM immediately after it receives a pair of qubits from both sides and classically communicates the BSM outcome to the neighboring repeaters. Let T_l be the time the last link qubit is emitted. The repeaters have all BSM outcomes at time $T_l + 2\tau_l$. This is when the repeaters know the measurement bases of all the logical qubits and, hence, all physical qubits in the tree codes. At this point, the logical X and Z measurements start at the repeaters. Note that, in our architecture, we assume that the indirect- Z measurement is non-adaptive. If we require a Z measurement outcome of a qubit at the repeater, irrespective of whether or not it is lost, we perform the indirect- Z measurement sequence on its children. This design choice avoids the delays in measurement caused by adaptive measurements, as discussed in Section VII C 1.

We now calculate the time at which the physical qubits of the tree code are measured. These times determine the

loss probability of the qubits. Consider a qubit i emitted at time T_i . If $T_l + 2\tau_l < T_i$, the photon is measured immediately. This is because the basis in which the repeater needs to measure qubit i is known prior to the emission of the photon. If $T_l + 2\tau_l > T_i$, qubit i has to wait for time $T_l + 2\tau_l - T_i$ before measurement. In other words, it is measured at $T_{mi} = \max(T_l + 2\tau_l, T_i)$. The amount of time the qubit waits before being measured or its *measurement wait time* is $T_{wi} = T_{mi} - T_i$.

The qubits emitted from the qubit chip with the spin emitters are first coupled into an optical fiber with efficiency η_c . These qubits keep undergoing losses in the optical fiber for their measurement wait times. The loss probability (l) of qubit i with measurement wait time T_{wi} is $1 - \eta_c \exp(-\alpha c_f T_{wi})$. Note that, unlike the all-photonic repeater protocols studied earlier [6, 10], the qubits in the RGS generated using the algorithm in Section V have different loss probabilities due to different wait times. We derive Pauli measurement success probabilities for tree code with non-uniform qubit loss probabilities using Section VII B.

3. Resource requirements

The RGS generation event starts with initializing the emitters and ends after all the photonic qubits have been generated and measured. Let T_{n_e} be the time required to generate one copy of the RGS using n_e emitters. Let τ be the repetition rate required by the protocol. We now calculate the number of emitters one would require to support the repetition rate $\tau < T_{n_e}$. Here, we use the concept of staggered generation, wherein to maintain the repetition rate τ , the repeater needs to start creating a new copy of the RGS at an interval of τ seconds.

The first RGS is generated using n_e emitters and the quantum repeater protocol starts at T_{n_e} . Up to time T_{n_e} , the repeater needs to employ $N_e = \lceil \frac{T_{n_e}}{\tau} \rceil n_e$ number of emitters for the staggered generation of RGS. At T_{n_e} , n_e emitters are measured, and the total number of emitters the repeater is actively using drops to $N_e - n_e = \lfloor \frac{T_{n_e}}{\tau} \rfloor n_e$. The measured n_e emitters then begin another round of RGS generation at time $\lceil \frac{T_{n_e}}{\tau} \rceil \tau$, increasing the number of emitters being used to N_e . To summarize, the repeater requires N_e emitters to produce an RGS every $T_{n_e} + k\tau$ seconds ($k \in \{0, 1, 2, \dots\}$), and attain the repetition time τ . This process is outlined in FIG. 12.

D. Results and discussion

In this section, we calculate the entanglement generation rate of our emitter-based all-photonic quantum repeater architecture and compare it with [10]. The RGS parameters are $\vec{b} = \{7, 3\}$ and $m = 4$ and we set $\tau = t_{\text{init}}$. At the minor nodes, we use linear optical BSM whose success probability is boosted to $3/4$ using ancilla qubits and

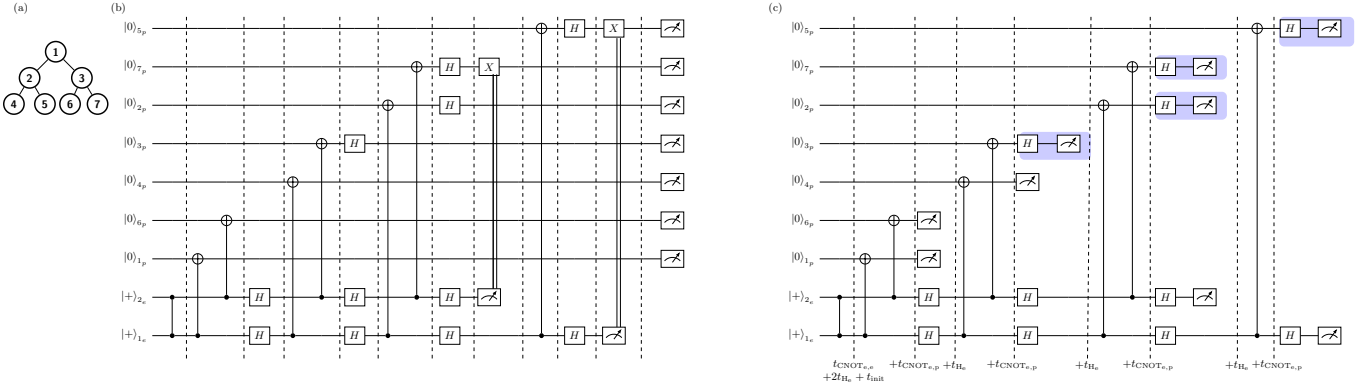


FIG. 11. Quantum circuit for graph state generation (a) tree graph state with $\vec{b} = \{2, 2\}$ (b) the quantum circuit to generate tree graph state on (a) using two emitters followed by measurement of photonic qubits in arbitrary Pauli bases. Operations between two dashed vertical lines are concurrent. (c) Simplified quantum circuit in (b) to minimize the qubit losses. The blue rectangles denote Hadamard-rotated measurements on the emitted photons. These measurements are instantaneous. The time needed to perform operations on the emitters between two dashed lines is noted below the lines.

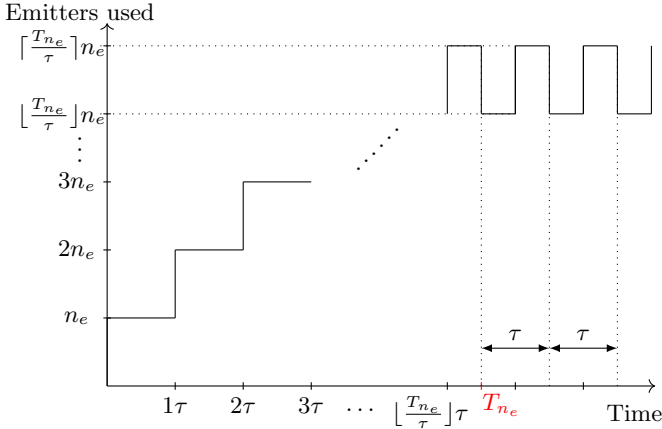


FIG. 12. Timing diagram for the number of emitters used at a repeater. One copy of the RGS is generated every τ seconds. The time required to generate the RGS using n_e emitters is $T_{n_e} > \tau$.

assume that the detectors are perfect. The emitter parameters are $t_{\text{cnot}_{e,e}} = 180\text{ns}$, $t_{\text{meas}} = 45\text{ns}$, $t_{H,n} = 15\text{ns}$, and $t_{\text{init}} = 15\text{ns}$. It is worth noting that these values are not specific to any particular hardware. They were chosen as an example to highlight the benchmarks needed for time scales before the emitter-based schemes improve upon the rates achieved without repeaters [15, 38–46].

For a given n_e , we first calculate the measurement wait times of all qubits in the RGS, followed by their loss probabilities as per the discussion above. The qubit emission times and measurement wait times are functions of n_e . Unlike the multiplexing method, the emitter-based method generates an RGS with different loss probabilities and, hence, different Pauli measurement probabilities for every logical qubit. As a result, we cannot use Eq 7 to calculate the entanglement generation rate. Instead, we perform a Monte Carlo simulation to calculate the

average rate for the emitter-based protocol. We begin by fixing n_e which in turn fixes N_e . For each L , we vary the number of repeaters n , and calculate the entanglement generation rate using Monte Carlo simulation. Then, to each L and n_e , we associate an entanglement generation rate maximized over n . In Fig. 13, for each L and n_e , we plot the maximum entanglement generation rate – also called the rate envelope. For the hardware parameters chosen, if the repeater generates RGS using the minimum number of emitters, given by the *height function* of the state [30], the entanglement rate is less than the repeaterless rate. In other words, it is better not to use repeaters altogether than to use only $n_e = 3$ emitters in the chosen parameter regime. However, if we increase n_e , our protocol beats the repeaterless rate as shown in FIG. 13.

Our protocol outperforms the multiplexing-based method (dotted red line in FIG. 13.) when $n_e \geq 40$. We calculate the number of emitters used by the multiplexing method to generate the RGS with probability ≈ 1 using the ‘improved multiplexing scheme’ from [10]. Note that, for this method, $N_e = n_e$. For the chosen hardware parameters, our emitter-based protocol is significantly more resource-efficient as it uses 1/40th of the emitters required by the multiplexing-based method to achieve an equal entanglement rate.

VIII. CONCLUSIONS AND FUTURE WORK

In this study, we have developed an algorithm for generating multi-qubit graph states using n_e -quantum emitters, where n_e is greater than the minimum number of emitters required. This algorithm delineates a sequence of Clifford operations, computational measurements, and photon emissions necessary for preparing specified graph states. The foundational elements of the algorithm are detailed in Section IV. Our algorithm is general for any

| Parameter | Symbol | Value |
|-------------------------------------|----------|------------------------------|
| Fiber loss coefficient | α | 0.046km^{-1} |
| Speed of light in the optical fiber | c_f | $2 \times 10^5 \text{ km/s}$ |
| Chip-to-fiber coupling efficiency | η_c | 0.99 |

TABLE I. Assumed hardware parameters

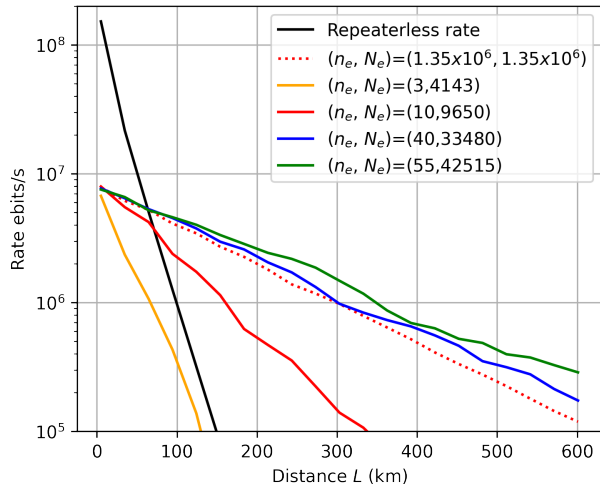


FIG. 13. Rate vs distance envelopes for when the RGS with $\vec{b} = \{7, 3\}$ and $m = 4$ is generated using emitters and multiplexing. n_e is the number of emitters used to generate one copy of the RGS, and N_e is the number of emitters required per repeater to achieve the repetition rate $\tau = t_{\text{init}}$.

graph state.

Another primary contribution is the assessment of resource requirements for generating repeater graph states. We demonstrate a trade-off between the CNOT circuit depth and the number of emitters, as illustrated in FIG. 8. This balance is crucial for understanding the efficiency of various graph states generation protocols.

A significant focus of our work is on the entanglement generation rates in all-photonic quantum repeaters. We introduce a new protocol tailored to graph states generated from quantum emitters, aiming to minimize the waiting time between photon emission and measurement. By integrating the timing dynamics of photon release from quantum emitters with this protocol, we calculate

entanglement generation rates under various parameters. In FIG. 13, we plot the envelopes the entanglement generation rates between Alice and Bob separated by a distance L . Our analysis emphasizes the necessity of optimizing both the graph state generation algorithm and the repeater protocol to surpass existing entanglement generation limits. Interestingly, our findings suggest that using a minimal number of emitters, such as three, is less effective. Our protocol, given specific experimental parameters, shows improved resource efficiency compared to multiplexing protocols. In conclusion, our work lays the groundwork for enhancing quantum repeater graph state generation, keeping in mind resource efficiency and entanglement rate optimization.

Looking ahead, we identify several avenues for further optimization. The ordering of primitives would be dependent on the objective function. We leave the optimality of the primitives for future work. In Section VD, we outline an algorithm to calculate the CNOT depth of the circuit obtained from the algorithm. The results are shown in Fig 8. Optimizing this algorithm for efficiency and effectiveness is a goal for subsequent research. An exciting line of work to explore would be to design an algorithm specifically for RGS that optimizes for the time of release of photon such that the loss experienced by the photon before being measured is minimized. This would involve not only optimizing for the order of primitives but also adding delays on the emitters in order to time the release of the photons to minimize loss.

ACKNOWLEDGMENTS

This work was funded by the Army Research Office (ARO) MURI on Quantum Network Science under grant number W911NF2110325. EK and AP acknowledge Prajit Dhara’s insights on the SiV vacancy center.

[1] P. W. Shor, Phys. Rev. A **52**, R2493 (1995).
[2] S. Bartolucci, P. Birchall, H. Bombin, H. Cable, C. Dawson, M. Gimeno-Segovia, E. Johnston, K. Kieling, N. Nickerson, M. Pant, F. Pastawski, T. Rudolph, and C. Sparrow, “Fusion-based quantum computation,” (2021), arXiv:2101.09310 [quant-ph].
[3] A. Kitaev, Annals of Physics **303**, 2 (2003).
[4] R. Raussendorf and H. J. Briegel, Phys. Rev. Lett. **86**, 5188 (2001).
[5] N. Sangouard, C. Simon, H. de Riedmatten, and

N. Gisin, Rev. Mod. Phys. **83**, 33 (2011).
[6] K. Azuma, K. Tamaki, and H.-K. Lo, Nature Communications **6** (2015), 10.1038/ncomms7787.
[7] N. Shettell and D. Markham, Phys. Rev. Lett. **124**, 110502 (2020).
[8] M. Varnava, D. E. Browne, and T. Rudolph, Phys. Rev. Lett. **100**, 060502 (2008).
[9] Y. Li, P. C. Humphreys, G. J. Mendoza, and S. C. Benjamin, Phys. Rev. X **5**, 041007 (2015).
[10] M. Pant, H. Krovi, D. Englund, and S. Guha, Phys. Rev.

- A **95**, 012304 (2017).
- [11] N. Shettell and D. Markham, *Phys. Rev. Lett.* **124**, 110502 (2020).
- [12] K. Nemoto, M. Trupke, S. J. Devitt, A. M. Stephens, B. Scharfenberger, K. Buczak, T. Nöbauer, M. S. Everitt, J. Schmiedmayer, and W. J. Munro, *Phys. Rev. X* **4**, 031022 (2014).
- [13] H. Choi, M. Pant, S. Guha, and D. Englund, *npj Quantum Information* **5** (2019), 10.1038/s41534-019-0215-2.
- [14] P. Dhara, D. Englund, and S. Guha, *Phys. Rev. Res.* **5**, 033149 (2023).
- [15] P.-J. Stas, Y. Q. Huan, B. Machielse, E. N. Knall, A. Suleymanzade, B. Pingault, M. Sutula, S. W. Ding, C. M. Knaut, D. R. Assumpcao, Y.-C. Wei, M. K. Bhaskar, R. Riedinger, D. D. Sukachev, H. Park, M. Lončar, D. S. Levonian, and M. D. Lukin, *Science* **378**, 557–560 (2022).
- [16] P. Dhara, N. M. Linke, E. Waks, S. Guha, and K. P. Seshadreesan, *Phys. Rev. A* **105**, 022623 (2022).
- [17] C. Schön, E. Solano, F. Verstraete, J. I. Cirac, and M. M. Wolf, *Phys. Rev. Lett.* **95**, 110503 (2005).
- [18] C. Schön, K. Hammerer, M. M. Wolf, J. I. Cirac, and E. Solano, *Phys. Rev. A* **75**, 032311 (2007).
- [19] N. H. Lindner and T. Rudolph, *Phys. Rev. Lett.* **103**, 113602 (2009).
- [20] J.-C. Besse, K. Reuer, M. C. Collodo, A. Wulff, L. Wernli, A. Copetudo, D. Malz, P. Magnard, A. Akin, M. Gabureac, G. J. Norris, J. I. Cirac, A. Wallraff, and C. Eichler, *Nature Communications* **11** (2020), 10.1038/s41467-020-18635-x.
- [21] I. Schwartz, D. Cogan, E. R. Schmidgall, Y. Don, L. Gantz, O. Kenneth, N. H. Lindner, and D. Gershoni, *Science* **354**, 434 (2016).
- [22] S. E. Economou, N. Lindner, and T. Rudolph, *Phys. Rev. Lett.* **105**, 093601 (2010).
- [23] J. Borregaard, H. Pichler, T. Schröder, M. D. Lukin, P. Lodahl, and A. S. Sørensen, *Phys. Rev. X* **10**, 021071 (2020).
- [24] D. Buterakos, E. Barnes, and S. E. Economou, *Phys. Rev. X* **7**, 041023 (2017).
- [25] Y. Zhan and S. Sun, *Phys. Rev. Lett.* **125**, 223601 (2020).
- [26] A. Russo, E. Barnes, and S. E. Economou, *Phys. Rev. B* **98**, 085303 (2018).
- [27] M. Gimeno-Segovia, T. Rudolph, and S. E. Economou, *Phys. Rev. Lett.* **123**, 070501 (2019).
- [28] H. Pichler, S. Choi, P. Zoller, and M. D. Lukin, *Proceedings of the National Academy of Sciences* **114**, 11362 (2017).
- [29] P. Hilaire, E. Barnes, and S. E. Economou, *Quantum* **5**, 397 (2021).
- [30] B. Li, S. E. Economou, and E. Barnes, *npj Quantum Information* **8** (2022), 10.1038/s41534-022-00522-6.
- [31] M. Varnava, D. E. Browne, and T. Rudolph, *New Journal of Physics* **9**, 203 (2007).
- [32] N. Sinclair, E. Saglamyurek, H. Mallahzadeh, J. A. Slater, M. George, R. Ricken, M. P. Hedges, D. Oblak, C. Simon, W. Sohler, and W. Tittel, *Phys. Rev. Lett.* **113**, 053603 (2014).
- [33] A. Patil and S. Guha, *arXiv preprint arXiv:2312.02377* (2023).
- [34] M. Varnava, D. E. Browne, and T. Rudolph, *Physical review letters* **97**, 120501 (2006).
- [35] M. Takeoka, S. Guha, and M. M. Wilde, *Nature Communications* **5** (2014), 10.1038/ncomms6235.
- [36] S. Pirandola, R. Laurenza, C. Ottaviani, and L. Banchi, *Nature Communications* **8** (2017), 10.1038/ncomms15043.
- [37] M. M. Wilde, M. Tomamichel, and M. Berta, *IEEE Transactions on Information Theory* **63**, 1792 (2017).
- [38] M. G. Dutt, L. Childress, L. Jiang, E. Togan, J. Maze, F. Jelezko, A. Zibrov, P. Hemmer, and M. Lukin, *Science* **316**, 1312 (2007).
- [39] W. Pfaff, T. H. Taminiau, L. Robledo, H. Bernien, M. Markham, D. J. Twitchen, and R. Hanson, *Nature Physics* **9**, 29 (2013).
- [40] D. Press, T. D. Ladd, B. Zhang, and Y. Yamamoto, *Nature* **456**, 218 (2008).
- [41] P. Thomas, L. Ruscio, O. Morin, and G. Rempe, *Nature* **608**, 677 (2022).
- [42] K. De Greve, P. L. McMahon, D. Press, T. D. Ladd, D. Bisping, C. Schneider, M. Kamp, L. Worschech, S. Höfling, A. Forchel, *et al.*, *Nature Physics* **7**, 872 (2011).
- [43] C. Nguyen, D. Sukachev, M. Bhaskar, B. Machielse, D. Levonian, E. Knall, P. Stroganov, R. Riedinger, H. Park, M. Lončar, *et al.*, *Physical review letters* **123**, 183602 (2019).
- [44] X. Rong, J. Geng, F. Shi, Y. Liu, K. Xu, W. Ma, F. Kong, Z. Jiang, Y. Wu, and J. Du, *Nature communications* **6**, 8748 (2015).
- [45] A. Gaëtan, Y. Miroshnychenko, T. Wilk, A. Chotia, M. Viteau, D. Comparat, P. Pillet, A. Browaeys, and P. Grangier, *Nature Physics* **5**, 115 (2009).
- [46] T. Wilk, A. Gaëtan, C. Evellin, J. Wolters, Y. Miroshnychenko, P. Grangier, and A. Browaeys, *Physical review letters* **104**, 010502 (2010).
- [47] F. Ewert and P. van Loock, *Physical review letters* **113**, 140403 (2014).

Appendix A: Implementation timescales in SiV color center emitters

In this section, we outline the method for applying a CNOT gate between two quantum emitters. We consider an electronic-nuclear spin system, where the nuclear spin serves as a deterministic long-lived memory qubit, such as SiV color centers. Each SiV color center consists of an electronic nuclear spin system. The electronic spin serves as the emitter and is used to emit photons of the graph state. From Section IV, CNOT on two emitters is a necessary operation to generate a graph state. In the SiV systems, the CNOT gate cannot be applied directly between two electronic spins. Moreover, the state of the nuclear spins cannot be measured. Taking these constraints into account, we outline the steps to apply a CNOT gate between two emitters in the state $|\psi\rangle_{e_1e_2}$, mediated through the nuclear spins, along with the parameterized time scales (refer FIG. 14):

1. The electronic spin states are stored in the corresponding nuclear spin states by applying a nuclear-electron swap gate [15], with time scales t_{SWAP} . This changes the state of the system to $|\psi\rangle_{n_1n_2} \otimes |?\rangle_{e_1e_2}$, where $|?\rangle$ implies some unspecified state.

2. The electronic spin is initialized in the ground state, with the time scales given as t_{init} . This changes the state of the system to $|\psi\rangle_{n_1 n_2} \otimes |00\rangle_{e_1 e_2}$.
3. Apply a Hadamard gate to the electronic spin. This is equivalent to rotating the electronic spin to a superposition of a ground state ($|0\rangle$) and an excited state ($|1\rangle$). To apply a Hadamard gate, a microwave pulse is applied to the electronic spin. The time scales are $t_{H,e}$. This changes the state of the system to $|\psi\rangle_{n_1 n_2} \otimes |++\rangle_{e_1 e_2}$.
4. Apply a laser pulse on the electron to obtain the state $|\psi\rangle_{n_1 n_2} \otimes \bigotimes_{j=1,2} (|01\rangle_{e_j p_{j,1}} + |10\rangle_{e_j p_{j,1}})$, where $j \in [1, 2]$, and takes time t_{ex} . Here, $p_{j,1}$ represents the photon emitted by electronic spin j and is in the single-rail encoding.
5. Apply an X gate to the electronic spin. The state of the electron-photon system is $|11\rangle_{e_j p_{j,1}} + |00\rangle_{e_j p_{j,1}}$. The time scales are $t_{X,e}$.
6. Apply another laser pulse on the electron to obtain the following electron-photon state $|110\rangle_{e_j p_{j,1} p_{j,2}} + |001\rangle_{e_j p_{j,1} p_{j,2}}$.
7. The state of the full system is now given as $|\psi\rangle_{n_1 n_2} \otimes \bigotimes_{j=1,2} |110\rangle_{e_j p_{j,1} p_{j,2}} + |001\rangle_{e_j p_{j,1} p_{j,2}}$. We rewrite the above state as $|\psi\rangle_{n_1 n_2} \otimes \bigotimes_{j=1,2} (|10\rangle_{e_j p_{j,L}} + |01\rangle_{e_j p_{j,L}})$, where we have used the dual rail encoding for the photonic qubits. The photons from each electronic system undergo a Bell state measurement (BSM) on the beamsplitter. Pauli X, Z corrections are applied to the electronic spins conditioned on the outcomes of the BSM. Entangling photons on the beamsplitter is probabilistic and instantaneous. To combat the probabilistic process, this whole process, starting from the initialization of the electronic spin is repeated till the Bell state measurement (BSM) succeeds. One attempt of photonic BSM takes time $t_{\text{ph}} = t_{\text{init}} + t_{H,e} + 2t_{\text{ex}} + t_{X,e}$. If p_{BSM} is the probability of success of the photonic BSM, the average number of trials required to get the first success is given by $1/p_{\text{BSM}}$. The detector inefficiencies can be folded into p_{BSM} [47]. The average time required to get the first BSM success is $t_{\text{BSM}} = t_{\text{ph}}/p_{\text{BSM}} + \max(t_{X,e}, t_{Z,e})$. Here, $\max(t_{X,e}, t_{Z,e})$ is the time taken to apply Pauli corrections on the electronic spin, and $t_{Z,e}$ is time to apply Pauli- Z gate on the electronic spin. If $|\psi\rangle_{n_1 n_2} \otimes |?\rangle_{e_1 e_2}$ is a stabilizer state, Pauli corrections affect only the phase of the state and can be tracked using classical computation. During this process, shown as the blue box in FIG. 14, the original state is stored in the nuclear spins and is not impacted by the failure of the Bell measurements.

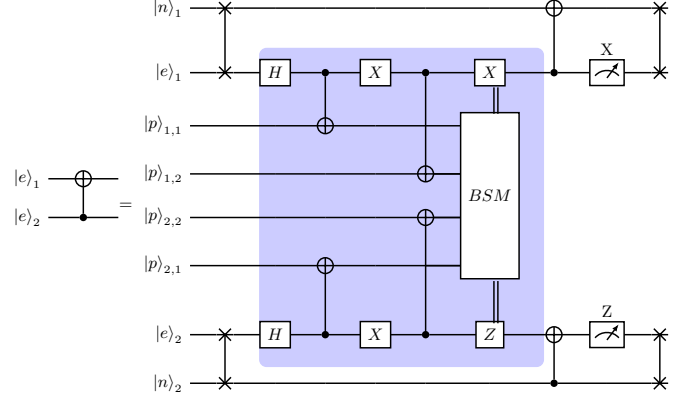


FIG. 14. The quantum circuit to perform CNOT between electronic spins of SiV centers, mediated through nuclear spins. The blue highlighted box represents generation of single photons using electronic spins, followed by BSM on the dual-rail photonic qubits (steps 2-7 in the text). As the photonic BSM is probabilistic, all processes in the blue box are repeated until the BSM succeeds.

8. Perform a CNOT gate on one of electron-nuclear spin pairs with nuclear spin as the control ($t_{\text{CNOT}_{n,e}}$) followed by Z measurement of the electronic spin that takes time $t_{\text{meas},z}$.
9. Perform a CNOT gate on the second nuclear-electron spin pair with the electron as the control qubits, with time scale given as $t_{\text{CNOT}_{e,n}}$ followed by the X measurement on the electronic spin, which takes $t_{\text{meas},x}$.
10. Swap the state of the nuclear spins with the electronic spins using swap gates.

The time taken to implement the CNOT gate between two quantum emitters $t_{\text{CNOT}_{e,e}}$ using the SiV vacancy center is given by -

$$t_{\text{CNOT}_{e,e}} = t_{\text{SWAP}} + t_{\text{BSM}} + \max(t_{\text{CNOT}_{n,e}} + t_{\text{meas},z}, t_{\text{CNOT}_{e,n}} + t_{\text{meas},x}) + t_{\text{SWAP}}$$

Appendix B: Emission times of photons

After setting up the circuit for the graph state generation, we assign a counter to each emitter c_{k_e} to keep track of the time of emission of the photon from each emitter and a pointer to keep track of the location in the circuit. Initialize all the time counters to 0 and initialize the pointer to the beginning of the circuit. The pointer moves along the circuit and encounters gates. Then, perform the following operations depending on the gate encountered by the pointer:

- Let $c_{k_e} = t$. The pointer associated with the k_e^{th} emitter encounters a H_e gate. Then the counter would be updated to $c_{k_e} = t + t_{H_e}$. That is, the time taken to implement the H_e gate is added to the time stored in the counter c_{k_e} .
- Let $c_{k_e} = t$. The pointer associated with the k_e^{th} emitter encounters a measurement of the emitter. Then the counter would be updated to $c_{k_e} = t + t_{\text{meas}} + t_{\text{init}}$.
- The pointer associated with the k_e^{th} emitter encounters a $\text{CNOT}_{e,e}$ gate, where the CNOT gate is between the k_e^{th} and the j_e^{th} emitter. Then, wait till the pointer associated with the j_e^{th} emitter also encounters the $\text{CNOT}_{e,e}$ between the k_e^{th}

and the j_e^{th} emitter. Let $c_{k_e} = t_1$ and $c_{j_e} = t_2$, and let $t_{\text{max}} = \max(t_1, t_2)$. Then, the counters are updated as follows: $c_{k_e} = t_{\text{max}} + t_{\text{CNOT}_{e,e}}$ and $c_{j_e} = t_{\text{max}} + t_{\text{CNOT}_{e,e}}$. The reason for introducing the variable t_{max} is that for the application of the $\text{CNOT}_{e,e}$ both the j^{th} and k^{th} emitters need to be ready.

- Let $c_{k_e} = t$. The pointer associated with the k_e^{th} emitter encounters $\text{CNOT}_{e,p}$ gate. Then the counter would be updated to $c_{k_e} = t + t_{\text{CNOT}_{e,p}}$. At this point, we associate the time stored in c_{k_e} with the emission time of the emitted photon.

The above steps output the time when the photons in the graph state are emitted.